Nuclear Materials and Energy 27 (2021) 100991

Contents lists available at ScienceDirect

Nuclear Materials and Energy

journal homepage: www.elsevier.com/locate/nme

Influence of thin tungsten oxide films on hydrogen isotope uptake and retention in tungsten – Evidence for permeation barrier effect

Kristof Kremer [a,b,*], Thomas Schwarz-Selinger [a], Wolfgang Jacob [a]

[a] Max-Planck-Institut für Plasmaphysik, D-85748 Garching, Germany
[b] Technische Universität München, 85748 Garching, Germany

ARTICLE INFO

Keywords:
Tungsten oxide
Permeation barrier
Thin film
Deuterium uptake
Deuterium retention
Thermal oxidation
Plasma irradiation
Tungsten
Deuterium

ABSTRACT

We studied the uptake of deuterium (D) into tungsten (W) through thin films of W oxide. Two surface oxide films with thicknesses of 33 and 55 nm were thermally grown on W substrates. In the following, the oxidized samples were exposed to low-energy D (5 eV/D) from a D plasma at a sample temperature of 370 K. A defect-rich layer of self-damaged W underneath the oxide was used as a getter layer to enable the detection of D that penetrates the oxide film. Depth-resolved concentration profiles of D and oxygen (O) were obtained after the plasma exposure by nuclear reaction analysis and Rutherford backscattering spectrometry. We have found that oxygen is partially removed from the first 100×10^{19} atoms/m^2 ($\approx$ 13.5 nm) of the oxide film by the D plasma which leads to a W enrichment in the near surface region. Independent of the oxide thickness, an oxygen removal rate of $(5.4 \pm 0.7) \times 10^{-4}$ O atoms per incident D atom was observed. Furthermore, D accumulates in the oxide film to concentrations of up to 1.3 at. %, but does not penetrate into the underlying self-damaged W. After a storage period of ten months at room temperature in vacuum, the D content in the oxide layer has decreased substantially, but still no D has penetrated into the metallic W. It is evident that surface oxide films on W effectively block the D uptake into metallic W. However, the D uptake into metallic W is not limited by the transport in the oxide film itself. D diffuses fast throughout the oxide but is stopped at the interface to the metallic W. We attribute this behavior to the difference in the heat of solution for D in W oxide and metallic W. D cannot overcome this barrier once it is thermalized to 370 K within the W oxide film.

1. Introduction

Tungsten (W) is a promising first-wall material for future fusion reactors, amongst other properties, due to its low hydrogen isotope (HI) retention. In the environment of a burning fusion plasma, however, the material will be subjected to large particle fluxes of ions and charge exchange neutrals from the plasma as well as high energy neutrons [1]. As a consequence of the neutron bombardment, defects are induced throughout the bulk of the material which increases HI retention [2]. Retention of HIs – especially of the radioactive tritium fuel – is not desirable, as retained tritium cannot contribute to reactor fueling and leads to a higher radioactive inventory.

In order to achieve a better fundamental understanding of the consequences that irradiation damage has for HI uptake, retention and release from W, dedicated laboratory studies have been carried out over the past years [2–10]. The overall goal of such experiments is to isolate individual aspects of HI retention in well-defined model systems to understand them independently as a bottom-up approach towards the full and more complex picture of HI retention in the first wall and divertor components of a fusion reactor. For practical reasons the overwhelming majority of these experiments is carried out "*ex situ*" meaning that the W samples have contact with ambient air before and in between experimental steps, e.g., between D plasma loading and ion beam analysis. Due to its affinity for oxygen, W readily forms a thin natural oxide film on the sample surface under ambient conditions [11]. Due to its low thickness of only 2–3 nm, this natural oxide film has not been taken into account for HI uptake, retention and release in W; see, e.g., [12,13].

Recently, however, a study by Hodille et al. [14] has indicated that these natural oxide films on W may have a significant effect on the release of HIs from W. This is an important point, as these natural surface oxide films are present in all *ex situ* laboratory experiments (and also in most *in situ* experiments if not great efforts are undertaken to remove them) but not in a fusion reactor, where they would most likely

* Corresponding author.
E-mail addresses: kristof.kremer@ipp.mpg.de (K. Kremer), thomas.schwarz-selinger@ipp.mpg.de (T. Schwarz-Selinger), wolfgang.jacob@ipp.mpg.de (W. Jacob).

https://doi.org/10.1016/j.nme.2021.100991
Received 22 December 2020; Received in revised form 23 February 2021; Accepted 28 March 2021
Available online 6 April 2021
2352-1791/© 2021 The Authors. Published by Elsevier Ltd. This is an open access article under the CC BY-NC-ND license (http://creativecommons.org/licenses/by-nc-nd/4.0/).

be reduced by the fusion plasma [15], at least for directly plasma-exposed surfaces. Therefore, any effects the natural oxide films might have would represent an unaccounted difference between laboratory studies and reactor relevant conditions. Clearly, a detailed understanding of the effects that natural oxide films have on the interaction of HIs with W is necessary to correctly interpret *ex situ* experiments and to enable the extrapolation of these results to reactor-relevant conditions.

The interaction of hydrogen with tungsten oxide (especially WO_3) has been extensively studied in the context of W-oxide-based gas sensors [16,17]. However, up to date there are only very few studies which are concerned with the effects of surface oxide films on HI uptake, retention and release in W, i.e., aspects relevant for the application of W as a first-wall and divertor material for nuclear fusion reactors. There are studies by Alimov et al. [18], Ogorodnikova et al. [19] or Addab et al. [20] who found increased deuterium (D) uptake and retention in the oxide films themselves, but these studies do not allow to draw any conclusion on the uptake, retention and release of HIs from/into bulk tungsten through the surface oxide films.

This present study aims to clarify which – if any – effects thin oxide films have on the uptake of D into the bulk of W samples. This question is approached by deliberately oxidizing W samples to surface film thicknesses of 33 and 55 nm. These oxide thicknesses were chosen because they are thick enough to yield a measureable effect, but still thin enough not to develop cracks. Thick oxide films (μm scale) are known to crack due to their volume difference compared with metallic W and data interpretation is then ambiguous [18].

The goal of this study is to a) investigate to what extent 33 to 55 nm thick oxide films affect D uptake into the underlying W and b) be able to draw conclusions about the effects of the thinner, natural oxide film that is almost always present in laboratory experiments.

To this end, a novel approach has been conducted: Thin oxide films have been thermally grown on top of MeV-ion-irradiated, defect-rich W. This defect-rich W acts as a getter layer for any HIs that possibly penetrate the oxide film into the metallic tungsten. The samples were then exposed to a low-temperature D plasma. Afterwards, the depth-resolved concentration of D and O was evaluated with ion beam analysis.

In the next section of this article the experimental setup and the analysis methods are presented, after that, the results are discussed in detail and then summarized. Lastly, the implications for HI uptake experiments are discussed and a conclusion is drawn.

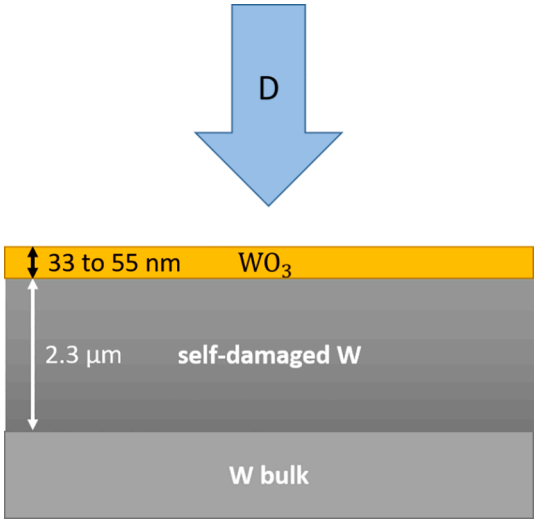

Fig. 1. Schematic of self-damaged and oxidized sample. The self-damaged zone (dark grey) acts as getter layer for D atoms permeating the surface oxygen film (yellow).

2. Experiment and analysis methods

The experimental approach is illustrated schematically in Fig. 1. The uptake of D from the plasma through the oxide film (yellow) into W is studied. As HI retention in pristine W is in general low [21,22] and, in addition, orders of magnitude lower than in tungsten oxide [13,18], the actual amount of D penetrating the oxide film and being retained in pristine W would be hard to determine. Therefore, we induce a 2.3 μm thick, defect-rich layer of so-called "self-damaged" W (dark gray) by bombarding the sample with 20.3 MeV W ions. This self-damaged region serves as a getter layer to locally enhance the D retention beneath the oxide film thus allowing a quantitative determination of the amount of D permeating through the oxide film into the metallic W. The depth-resolved D content in the sample and the depth-resolved oxygen (O) concentration in the oxide film are measured *ex situ* by ion beam analysis (IBA) after the plasma exposure.

2.1. Sample preparation

Six W samples are used in this study. They are cut from a single sheet of hot-rolled W with a purity of 99.97 wt. % supplied by Plansee [23]. All samples are 15 × 11.8 × 0.8 mm^3 in size.

First, the sample surface is mechanically grinded and then electropolished in 1.5% NaOH to achieve a mirror-like finish [24]. The samples are then cleaned in an ultrasonic bath first with acetone then with isopropanol for 20 min each. Afterwards they are rinsed in distilled water and remaining water droplets are removed with an air blower.

Next, the samples are annealed by electron-beam heating in ultra-high vacuum (base pressure $< 10^{-9}$ Pa, rising to $<3 \times 10^{-5}$ Pa during annealing) at 2000 K for 5 min. This reduces the defect density in the bulk and thus minimizes its contribution to the total HI retention in the sample. Additionally, the heating allows grain growth to a diameter of ≈10–50 μm (see Figs. 2 and 3), which minimizes the possible effects of grain boundaries on HI retention.

Afterwards, the samples are irradiated with 20.3 MeV W^{6+} ions at 300 K at the IPP tandem accelerator laboratory in Garching. The ion beam is scanned across the sample surface to achieve a laterally homogenous irradiation at a fluence of 7.87 × 10^{17} W/m^2. This creates a "self-damaged" zone in the first 2.3 μm of the W sample with a maximum

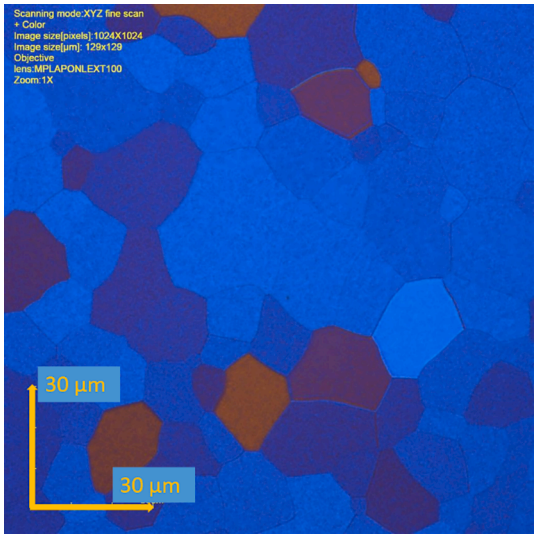

Fig. 2. Digital, optical microscopy image of the W sample with thick oxide. The different grain heights are illustrated by the color difference that stems from light interference in the transparent oxide film. Most grains have a similar thickness near to the maximum oxide thickness of 55 nm (blue). Only a few grains are less thick (orange). The thickness distribution ranges from 30 to 55 nm.

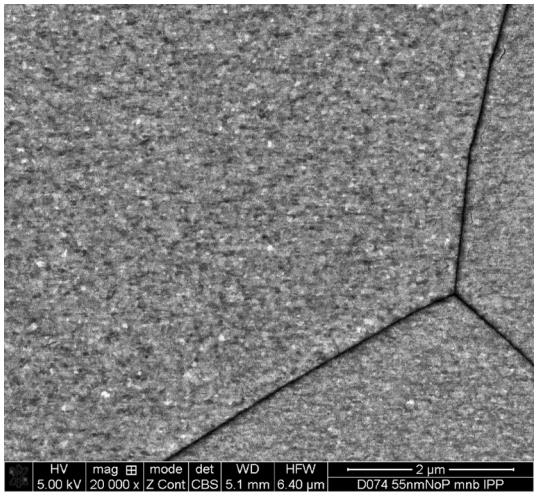

Fig. 3. SEM image of the thick (55 nm) oxide film on W sample from backscattered electrons in Z contrast. Three W grains are shown. The nanocrystalline structure of the oxide film is visible.

calculated displacement damage of 0.23 displacements per atom (dpa) [25]. This step is essential for the experiments as the self-damaging introduces a well-controlled amount of defects in the material without changing the elemental composition. These defects later act as traps for HIs which significantly enhance the HI retention in the self-damaged W, so that the total HI retention in the sample is now governed by the self-damaged zone. Furthermore, HIs that are bound in these traps can no longer diffuse at room temperature [3,26] and are thus retained for later measurements of the HI amount and depth profile with ion beam analysis. The self-damaged zone is, hence, used as a "getter layer" that accumulates HIs that permeate through the oxide film.

2.2. Oxidation and characterization of the oxide film

After self-damaging, four samples are oxidized thermally at 600 K in a vacuum thermo-gauge in a mixture of 80% argon and 20% oxygen at atmospheric pressure. Two pairs of samples with different oxide thicknesses are prepared: 33 nm corresponding to 12 h of oxidation time and 55 nm corresponding to 36 h. We refer to these samples as thin and thick oxide in the following. A relatively low temperature of only 600 K for oxidation was chosen in order to minimize thermal annealing of the defects in the self-damaged zone [27,28].

As pointed out e.g. in [31] the tungsten-oxygen system is rather complex. Besides the stable oxides WO_3, $WO_{2.9}$, $WO_{2.72}$, and WO_2 a variety of non-stoichiometric compounds exist. However, at temperatures between 290 and 600 K monoclinic γ-WO_3 is expected to grow [31]. The thick oxide film was investigated with sputter X-ray photoelectron spectroscopy (XPS). The measured XPS peak positions as well as the stoichiometry (determined from the relative intensities of the W 4f and O 1s peak integrals) are compatible with an assignment to WO_3 (compare [29]). This stoichiometry is also in agreement with RBS measurements (see Section 3.1). However, we cannot exclude with certainty the presence of non-stoichiometric oxides that are very close to WO_3. The possible contribution of such sub-oxides to the XPS signal is estimated to be below 10 at.%. No hints of other impurities were found in the XPS analysis, after the topmost surface layer of adsorbates was removed by argon sputtering. The sensitivity for detection of other species is estimated to be <1 at.%. The measured XPS spectra are shown in the supplementary material (S5).

An additional pair of reference samples is subjected to the same temperature profile (i.e., exposure to 600 K) in the same oven, but without oxygen (100% Argon atmosphere). Thus, it experiences the same amount of defect annealing as the thermally oxidized samples, but does not grow an additional oxide. However, the natural oxide present before the annealing remains on the sample since the annealing temperatures are not high enough to desorb tungsten oxide [30,31].

Aside from XPS several independent methods were used to characterize the oxide films with respect to their thickness, their oxygen amount and their behavior upon interaction with D ions from a plasma:

a) By direct measurement of the oxide film cross section from a focused ion beam (FIB) cut. The images were prepared with a scanning electron microscope (SEM - model FEI HELIOS NanoLab 600).
b) By laser ellipsometry (Jobin Yvon PZ 2000 operating at 632.8 nm with a 10 µm × 505 µm spot size).
c) By ion beam analysis (IBA) with nuclear reaction analysis (NRA) and Rutherford backscattering (RBS). These methods are described in detail in Sections 2.4 and 2.5, respectively.

Ellipsometry measurements of the natural oxide layer and the thick oxide layer were performed before and after plasma exposure. This technique measures the polarization change of light that is reflected from the sample surface to determine the refractive index and the optical film thicknesses. To interpret the data (the complex reflectance ratio of the material, expressed as an amplitude component Ψ and a phase component Δ), an optical model of the layer system on the sample is needed. Besides the film thickness this model requires knowledge of the optical constants of the layers. These optical constants are known for W and for tungsten trioxide (WO_3) [32].

Note, however, that the growth rate of thermally grown WO_3 on W depends on the crystal orientation of the W substrate [33,34]. Its thickness is, therefore, varying between different grains of the polycrystalline W substrate. The mean diameter of the W grains in our samples is approximately 10–50 µm, as is shown in Fig. 2. According to energy dispersive x-ray spectroscopy (EDX) mapping and FIB cross sections by K. Schlüter [35] on thermally oxidized W samples at different oxide thicknesses using the same W grade that is used here, most W grain orientations grow a very similar oxide thickness close to maximum thickness and only a few W grain orientations grow thinner oxides down to 60% of the maximum thickness. This thickness distribution is assumed to scale linear with oxide film thickness and is assumed for both the thin and the thick oxide (33 and 55 nm). It is used in this work for the simulation of the oxygen depth profiles with RBS (see Section 2.5).

The grain-dependent thickness of the thicker (55 nm) oxidized sample is visualized with a digital microscopy image (LEXT OSL4000 by Olympus) in Fig. 2. The color features stem from light interference in the transparent oxide film. Most grains are close to the maximum thickness of 55 nm (blue) and only a few show a lower thickness (orange), which is in agreement with the above mentioned distribution measured by K. Schlüter [35].

Furthermore, Fig. 3 shows a top view scanning electron microscope (SEM) image of the sample surface using a backscattered electron detector (Z contrast). Three different W grains are visible underneath the oxide film. They have an average grain size of about 10–50 µm. Distinct grooves at the grain boundaries (dark lines) are formed during the heat treatment at 2000 K before oxidation. The oxide film itself is visible on top of the W grains. It has a much smaller, nano-crystalline structure, with an average grain size of about 10–50 nm.

2.3. Deuterium plasma exposure

Three samples with different oxide thicknesses (33 nm, 55 nm and the reference sample with only the natural oxide film) are simultaneously exposed to a low-temperature D plasma in the plasma device "PlaQ". A detailed description of the setup is given in Ref. [36,37]. PlaQ provides highly reproducible, temperature-controlled, low-energy D exposure. Up to six samples can be exposed radially symmetric on a single sample holder to ensure identical plasma-loading conditions. The

sample holder has a feedback-controlled temperature regulation by a liquid thermostat. In this experiment, the sample temperature is kept at 370 K. It is independent from the plasma flux.

To avoid implantation of the D ions deep into or even through the oxide film, a low D ion energy is desirable. To achieve such "gentle" plasma loading conditions the sample holder is left at floating potential to minimize the potential difference between plasma and sample. This results in an ion energy of about 15 eV. The majority of the ion flux in PlaQ consists of D_3^+ (94%) with a minority of D_2^+ and D^+ (3% each). We assume that for molecular ions (D_3^+, D_2^+) the energy is shared evenly between the D atoms upon contact with the sample surface. Thus, we refer to this conditions as low-energy (<5eV/D), "gentle" plasma exposure.

We expect the temperature as well as the ion energy to be of vital importance for D-WO_3 interaction. Here, we have chosen one specific condition – i.e., a gentle plasma exposure at 370 K - because many *ex situ* D uptake and retention studies in (self-)damaged W were performed under similar conditions, e.g., [3,4,25]. The moderate temperature is high enough to allow for good D mobility in W and low enough to avoid annealing of the displacement damage that was introduced during the self-damaging. The low D ion energy is below the damage threshold of W and prevents the creation of additional defects in the material [5]. Restrictively, it should be mentioned that it is not a priory clear if this assumption also holds for W oxides.

For D loading the plasma chamber is first cleaned of impurities by a 15 min "burn in" phase where a shutter prevents the plasma from interacting directly with the samples. During this phase only atomic D can reach the samples via gas phase collisions or by collisions with the chamber walls. Then, the shutter is opened and the samples are exposed to an ion flux of 5.6×10^{19} D/m^{2}s. After seven hours of exposure time this accumulates to a total fluence of 1.4×10^{24} D/m^2.

2.4. D areal density and D depth profile

Ion beam analysis was used to determine the depth-resolved concentration profile of D atoms in the sample – the so called "D depth profile" [38]. The measurements were performed *ex situ*, first two days after plasma exposure and then again after ten months of sample storage in a desiccator. To quantify D, the nuclear reaction D(^{3}He,p)α was exploited. By using ten different incident ^{3}He ion energies, ranging from 500 to 4500 keV, one can measure the D concentration in the sample to a depth of up to 7.4 μm. This easily covers the interesting regions of the sample, i.e., the surface oxide film and the 2.3 μm of self-damaged W.

The protons were detected by a Si(Li) annular detector with a solid angle of 19.5 ± 0.5 msr. The detector circularly encloses the ion beam at a laboratory scattering angle of 175°. This allows for a depth resolution at the surface of 54 nm for pure W or 80 nm in WO_3. Note that the depth resolution of NRA measurements depends on the stopping power of the involved particles in the material. Since the density of the WO_3 oxide film (7.16 g/cm^3 [39]) is much smaller than that of pure W (19.25 g/cm^3) the depth resolution in the WO_3 oxide film is lower than in pure W. All depth resolutions were calculated with the program "ResolNRA" [40] using SRIM stopping powers [41].

For ^{3}He energies below 1200 keV the alpha particles from the D (^{3}He,α)p nuclear reaction can contribute information about the D concentration in the near surface region. Measuring the alpha particles with a passivated implanted planar silicon (PIPS) detector with a solid angle of 7.65 ± 0.26 msr at a laboratory scattering angle of 102° gives an information depth of approximately 0.3 μm in W. As the stopping power of alpha particles in W or WO_3 is higher than that of protons, this method also provides a better depth resolution of 27.5 nm (pure W) or 50 nm (WO_3) throughout the oxide film.

The programs "SIMNRA" [42] and "NRADC" [43] were used to deconvolute the D spectra of the different ^{3}He energies for D depth profiling. NRADC uses the proton and α spectra at all measured energies as input to construct the most likely distribution of D atoms across the sample depth. A detailed description can be found in Ref. [43]. The cross section data from Besenbacher and Möller [44] was used for the alpha spectrum and the cross section data from Wielunska et al. [45] was used for the proton spectra. Both cross section measurements have a total uncertainty of <±5%. To monitor detector performance and to optimize the energy calibration of the detectors, a thin film of plasma-deposited, amorphous, deuterated hydrocarbon (a-C:D) on a silicon substrate was used as calibration sample and was measured at each energy [45,46]. As the deuterium containing a-C:D surface layer is very thin, stopping in the a-C:D layer is negligible. Thus, the resulting peaks from the D(^{3}He, p)α reaction – and in addition the ^{12}C(^{3}He,p)^{14}N reaction above 2 MeV – are very sharp and can be used to perform an energy calibration for each incident ion energy. The accuracy of the ion beam current measurement is typically within 3–5% and together with the statistical error of approx. 1% (depending on the ion dose, ion energy and D concentration in the sample), the reproducibility of the NRA measurement stays within 5% relative to each other.

2.5. Oxygen areal density and oxygen depth profile

A further application of the ^{3}He ion beam stems from the interaction with oxygen via the reaction ^{16}O(^{3}He,p$_0$)^{18}F. This reaction allows to directly measure and quantify the areal density of oxygen in the surface oxide film. The cross section of this reaction was recently measured [46] and has an absolute accuracy of 4.7% at an energy of 4000 keV of the incident ^{3}He ions. This energy was used for all NRA oxygen measurements here, since the cross section is flat in this energy range. Therefore, uncertainties in the incident ion beam energy cause only a small change of the cross section [46]. The energy loss of the ^{3}He ions due to stopping in the oxide is small and can be neglected. The maximum probing depth is determined by the stopping of the incident ^{3}He ions in the WO_3/W material and is in the range of several μm, i.e., much larger than the oxide film thickness. Thus, the areal density of oxygen in the oxide film is reliably measured by this method for our samples. On the other hand, this high penetration depth is associated with a low depth resolution at the surface. Therefore, this method cannot yield a depth-resolved concentration profile of the oxygen atoms in the oxide film, but gives only the total areal density of oxygen on the sample. From the areal density of O atoms the corresponding thickness of the oxide film in nm (stated above as 33 nm and 55 nm for the oxidized samples) can be derived under the assumption of stoichiometric WO_3. The literature values for the density of WO_3 vary between 6.87 [47] and 7.3 g/cm^3 [31]. Here we assume a density of 7.16 g/cm^2 according to [39]. The protons from the nuclear reaction with oxygen are measured with a Si(Li) detector with a solid angle of 78.7 ± 0.5 msr at a scattering angle of 135°. To determine the areal density of oxygen in the sample, the background-subtracted integral of the proton peak is taken, and compared with SIMNRA [42] simulations.

Additionally, RBS measurements were conducted with ^{4}He ions. This is realized by a PIPS detector that is positioned at a scattering angle of 165° in Cornell geometry and has a solid angle of 1.108 ± 0.038 msr. The RBS measurement provides another independent method to quantify the areal density of oxygen in the sample. But the real strength of the method is its ability to determine the oxygen depth profile of the surface oxide film, i.e., the oxygen concentration at different depths within the oxide film. Note, however, that oxygen on a W substrate cannot be directly detected by RBS measurements. The energy of the recoiled He ions depends on the atomic masses (Z) of projectile and target atoms. Therefore, He ions that are scattered from oxygen have far less energy than He ions scattered from W atoms. As, additionally, the RBS cross section is proportional to Z^2, the oxygen signal is much lower than the W signal. Consequently, the low O signal at low energy is superimposed by a huge W background and not quantifiable. The information of the oxygen depth profile appears indirectly, however, in the RBS spectrum as a "lack of W signal intensity" at high recoil energies. This is illustrated in Fig. 4, where the RBS spectrum (^{4}He ions at 800 keV) of the 55 nm thick

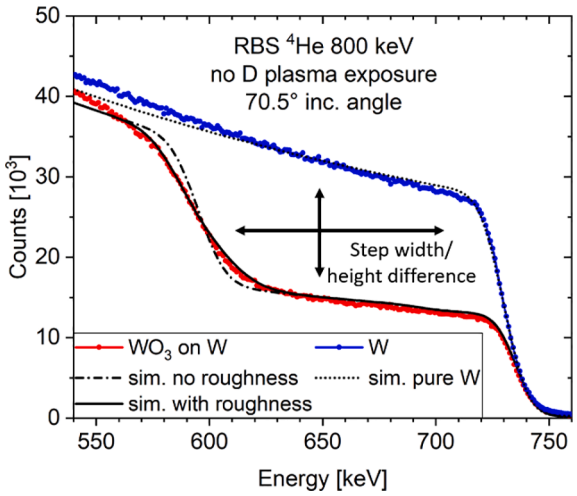

Fig. 4. RBS spectra of W with natural oxide (blue) and with the 55 nm thick oxide film (red) before plasma exposure.

oxide film on W (red) is compared with the spectrum of a W sample with only natural oxide (blue); both before plasma exposure. The RBS spectrum of bulk W of the natural oxide sample exhibits a single step at about 730 keV followed by a continuum towards lower energies. The surface oxide film of the thick oxidized sample exhibits two steps; a first step of lower intensity ranging from 730 to about 600 keV that marks the oxide film and a second one at about 575 keV that marks the transition to metallic W.

He ions scattering at W atoms at the very surface of the sample are recoiled with the highest energy. Ions that penetrate deeper into the sample before being recoiled lose energy on their way in and out by electronic stopping. The energy scale can, therefore, be interpreted as a depth scale into the sample. From the width of the "first step" in the spectrum of the oxidized sample, the W and O areal densities of the oxide film can be deduced. From the height difference between the two spectra at a certain energy, the difference in the oxygen concentration in a certain depth can be inferred. It is worth noting that scattering/recoiling of the He atoms on the O atoms is not the reason for the reduced W intensity within the oxide. The dominant cause for the lower intensity in the surface oxide (above about 600 keV) is the additional electronic stopping from the O atoms. This additional, statistical energy loss in between W atoms "stretches" the number of recoiled He atoms over a wider energy region. Thus the number of counts per energy interval is decreased within the oxide layer. An illustrative example of this phenomenon can be found in the supplementary material (S1). Note that the absolute height (counts per ion dose) of the spectrum does not only depend on the composition of the sample at this depth but also on the composition closer to the surface that the ions have to go through to be detected. Thus, absolute heights of different spectra are not directly comparable and a simulation with, e.g., SIMNRA [42] is necessary for quantitative interpretation of the sample composition. It is also important to note that the corresponding concentration of O atoms at a given depth can only be deduced in this way when assuming that there are no other impurities present in the material. This assumption is valid here, as only negligible amounts of other light elements (e.g., carbon <1 at.%) have been found on the sample with NRA, XPS and EDX measurements.

To obtain the RBS spectrum in Fig. 4, the sample was rotated such that the surface normal forms an angle of 70.5° with the line of the incident ion beam. By this the geometric path of the ions through the oxide film, and hence the depth resolution of the RBS measurement, is enhanced by a factor of three. With RESOLNRA [40] the calculated depth resolution in the oxide film is 43×10^{19} atoms/m^2 at the surface and 53×10^{19} atoms/m^2 at the deepest part (55 nm) of the thick oxide film. For the evaluation of the RBS spectra an average depth resolution of $\leq 50 \times 10^{19}$ atoms/m^2 was applied for the oxide film.

The modeling of the depth-resolved oxygen concentration in the sample is realized by the fitting program "MultiSIMNRA" [48]. It uses multiple instances of SIMNRA [42] (version 7.02) to simulate RBS spectra at different energies and varies the target elemental composition to give the best fit to the experimental data. In MultiSIMNRA the oxide film is divided into several sublayers with constant composition. The layer thickness is set equal to the depth resolution of the RBS measurement (50×10^{19} atoms/m^2). The concentration of O and W atoms in these sublayers is then varied to optimize the fit to the experimental spectrum.

Simulation results for a pure W sample as well as for WO_3 consisting of 385×10^{19} atoms/m^2 on top of tungsten are shown in Fig. 4. The agreement between experiment and simulation is very good. It is important to note that the size of the analyzing beam spot of 1 mm^2 is larger than the mean W grain size of 10–50 μm. Hence the beam averages over many grains with different oxide thicknesses. In SIMNRA such variation in film thickness can be described by defining a sublayer of constant composition with a so-called "layer roughness". The influence of this thickness variation is also shown in Fig. 4 were two cases are compared: A smooth oxide film (no roughness) with one where the known oxide thickness distribution is taken into account [35]. It is clear that the model with roughness provides a far better fit to the experimental data. We want to stress here that the thickness variation affects only the left part of the lower intensity step in the RBS spectra, i.e., the deepest part of the oxide films. As can be seen in Fig. 4 the high energy and hence surface near part of the spectrum is unaffected. This holds true as long as the scattered ^{4}He does not encounter the underlying metallic substrate. Once this happens a gradual transition from the oxide film to the underlying W substrate leads to a smearing out of the step in the RBS spectrum in this energy region. In general, the same effect would be observed if an oxygen concentration gradient in the film would be present. However, in the case of Fig. 4 the assumption of a gradient is not necessary as the known roughness distribution describes the measured spectrum very well.

RBS measurements were performed for all samples before and after plasma exposure and the corresponding oxygen areal densities and depth profiles were determined. The results are discussed in Section 3.1.

3. Results and discussion

3.1. Oxide reduction and oxygen removal by the deuterium plasma

Here the results of several independent measurement methods for the oxide film thickness, the oxygen areal density and the stoichiometric composition of the oxide are presented. The changes of the oxide film before and after plasma exposure are discussed and a comprehensive picture of the evolution of the oxide film under plasma exposure is drawn.

3.1.1. SEM and ellipsometry

SEM: Direct measurements of the cross section of the thick (55 nm) oxide film were performed before and after plasma exposure. The two different cross sections were prepared via a FIB cut in an SEM and are shown in Fig. 5. As the surface normal of the sample is tilted by 52° to align with the FIB, the cross section is tilted by 38° relative to the electron beam. Therefore, the vertical scale in the shown SEM image is compressed by a factor $\cos(38°) = 0.79$. Fig. 5a) shows a part of the FIB cross section before plasma exposure. The oxide film is visible between the W grains (at the bottom) and the protective coating for the FIB cut on top. The oxide film appears to be smooth, coherent and no porosity is visible. The thickness of the oxide film is then directly measured across three different W grains (only two are shown in the image). The average thickness of the oxide film determined by this method is 53.9 ± 1.5 nm, which agrees well with the nominal bulk density of WO_3 when compared to the oxygen amount measured with NRA and RBS (see

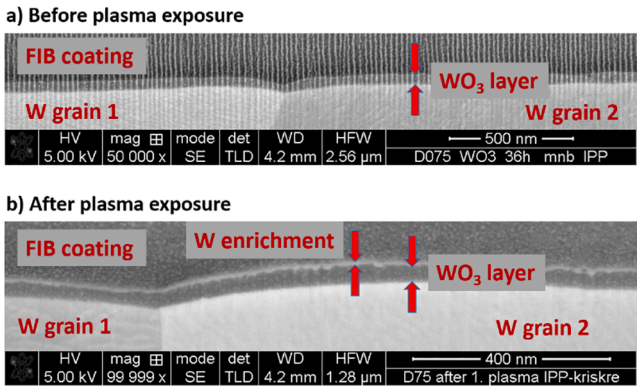

Fig. 5. SEM images of two different FIB cross sections through the thick (55 nm) oxide film a) before plasma exposure and b) after plasma exposure (please note the different magnification in both images).

Section 3.1.2). Note, however, that due to the small size of the observation area the image contains only three W grains. This is not necessarily representative for the full, grain-orientation-dependent thickness distribution. The average thickness of the three individual grains measured here varied between 42.3 ± 1.2 nm and 59.2 ± 0.9 nm. Fig. 5 b) shows a different cross section on the same sample after plasma exposure; note the two times higher magnification. On top of the oxide film a bright line is visible which indicates a material of higher Z number. This is interpreted as a thin, W-enriched layer of at least partially reduced WO_3.

Ellipsometry: The results of the ellipsometry measurements of the oxide thickness are shown in the Psi-Delta graph in Fig. 6a). The gray dots depict the natural oxide film before oxidation and the blue ones depict the results after the sample was oxidized to a thickness of 55 nm and then plasma exposed. The measurement positions for the natural oxide are distributed across the whole sample surface size (15 × 12 mm) in a rectangular grid. As the sample surface is not perfectly plane but slightly domed after polishing, the mismatch between the incident angle of the laser and the local surface normal leads to a scattering of the data. The measurement of the oxidized sample is performed on a much smaller region of the sample and thus the scattering is less pronounced. It covers an area that was partially masked by a screw fixing the sample on the sample holder during plasma exposure. A map of the scanned area is shown in Fig. 6b). The data band on the right of the blue dots (Psi values larger than 35°) marks unreduced WO_3 that was protected from the plasma by the screw head (green & red region in Fig. 6b)). The blue data cloud on the left (Psi = 22° to 29°) stems from an area on the sample that was exposed to the plasma (blue area in Fig. 6b)). In addition to the experimental data, two different simulations are shown (red and green in a)). They consist of an optical model of the metallic W substrate with a layer of WO_3 on top. Each dot in the simulated spectrum corresponds to a thickness increase of 1 nm of the respective material. The red curve starts with pure W (at about Psi = 25°) extending to 55 nm of pure WO_3. The green curve starts at 42 nm of (remaining) WO_3 which is covered with up to 3 nm metallic W. The red model is in agreement with the assumption that underneath the screw still WO_3 of the original thickness (55 nm on average) exists. Note that the measurement spot size is 10 µm × 30 µm and hence comparable to the grain size. Therefore, the data points are spread along the red model curve due to the grain-dependent thickness of the oxide film. Some data points of thicker than average oxide films even extend further to the right of the model curve. The data cloud on the left side of the plot after plasma exposure (corresponding to the area not protected by the screw) cannot be explained by WO_3 alone. Otherwise, it would be located along the red model line. This data can be described by a reduced WO_3 thickness (of 42 nm) with a 3 nm thick cover layer of pure W on top. This is shown as the green branch of the model. It is not possible to simulate a layer of partially reduced W oxide (e.g. WO_2), as no optical model for this is available. Thus it cannot be concluded from ellipsometry whether a full reduction of WO_3 to W or a partial reduction of WO_3 to W sub-oxides (e.g., WO_2) takes place. Nevertheless, these ellipsometry measurements suggest that oxygen is removed by the plasma leaving behind a W-enriched zone at the surface.

3.1.2. *Oxygen areal density*

The oxygen areal density and the oxide thickness were determined by ion beam analysis by using the $^{16}O(^3He,p_0)^{18}F$ nuclear reaction (NRA) or backscattered ^4He ions (RBS), as described in Section 2.5. Fig. 7 shows the result for the thin (initially 33 nm) and thick (initially 55 nm) oxide films derived from measurements with NRA (blue) and RBS (red). For both samples the oxygen areal density before and after plasma is shown, as well as the difference between this two values. The NRA and RBS measurements of the thick oxide were performed on the same sample before and after plasma. The RBS measurements of the thin oxide were performed on two samples with nominal identical oxide thickness (identical samples oxidized for the same time under the same conditions) of which only one was plasma exposed.

From both NRA and RBS measurements, it is evident that a substantial amount of oxygen is lost from the sample during plasma exposure. Both methods agree very well and the amount of lost oxygen from the NRA measurements is reproduced by the RBS measurement within the error bars of the methods. The numeric values from the NRA and RBS measurement are given in Tab. S1 in the supplementary material (S2).

Furthermore, the loss of oxygen during plasma exposure is roughly

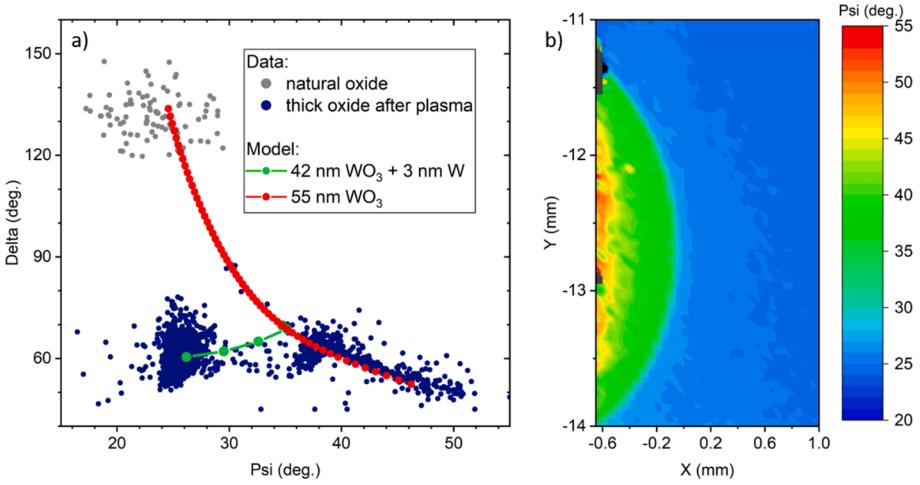

Fig. 6. a) Ellipsometry measurement of the natural oxide film (gray) and the thick oxide film after plasma exposure (blue). Part of the scanning area was covered by a fastening screw during plasma exposure and was not affected by the plasma. This is illustrated in b), showing the lateral variation of Psi of the corresponding section of the sample. The unaffected part of the thick, thermally grown oxide (green & red area in b)) and the natural oxide can be modeled as a WO_3 film on top of W substrate (red curve in a)); the plasma exposed part of the thick oxide (blue color in b)) can be modeled by a 40 nm oxide film on W with a 3 nm thick metallic W cover layer on top of the film (this metallic W layer is represented by the green curve in a)).

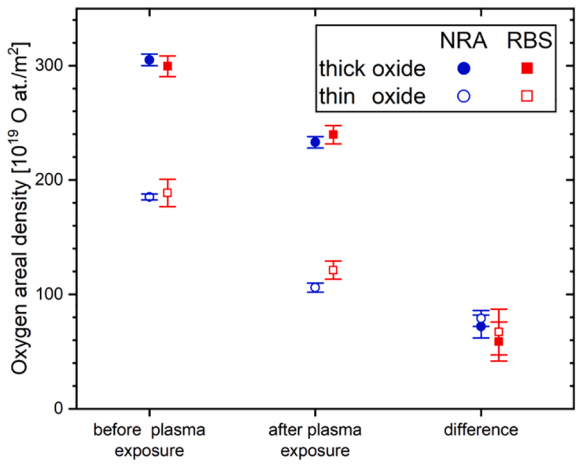

Fig. 7. Comparison of the oxygen areal density before and after plasma exposure for the thin and thick oxide samples. Both measurement methods (NRA and RBS) agree within the experimental uncertainty. Although the original oxide thicknesses vary, the absolute difference (oxygen loss during plasma exposure) is the same for both samples.

equal (difference <10%) for the two oxidized samples. Hence, it seems to be independent of the initial oxide thickness. This indicates that the oxygen removal process takes place mostly from the surface of the oxide film and is not a volume effect. This is noteworthy, since D is highly mobile in WO_3 and is expected to diffuse inside the polycrystalline oxide film within minutes at room temperature [49,50]. Furthermore, this D uptake leads to a color change of the oxide [20,30,50]. Indeed, we observed first a rapid color change of the oxide film within the first minutes of D plasma exposure (and also during the "burn in" phase were only atomic D can reach the sample), and then a second slower color change over the course of several hours of plasma exposure (see video in supplementary material (S3)). We attribute the first (fast) color change to the intercalation of D atoms into the WO_3 and the formation of tungsten bronze (D_xWO_3), which changes the optical properties of the oxide film. The fast color change has previously been reported, e.g., by Addab et al. [20] for similar conditions. It is also utilized commercially for gas sensors based on tungsten oxides [16,17]. Note, however, that for these gas sensors a thin catalyzer (Pd or Pt) is used on the surface to dissociate the D_2 molecules into atoms, before they can enter the oxide. We have also not observed any color change during D_2 gas exposure prior to the "burn in" phase and the plasma exposure. The formation of tungsten bronze, and thus the color change, is expected to be slowly reversible during storage at room temperature [20] and indeed, we observed a color change over several weeks after plasma exposure. The second, slower color change observed during plasma exposure is, in contrast, attributed to the gradual removal of oxygen from the oxide layer in the surface-near region by the plasma. Such a removal of oxygen from tungsten oxide has been previously observed by Hopf et al. [15], although in a hydrogen plasma with much higher ion energies of 200 to 400 eV compared to our <5 eV/D "gentle" D plasma. The oxygen loss and thus the thinning of the oxide film permanently changes the interference color of the film. The slow color change, thus, comes in addition to the fast color change induced by the intercalation of D atoms. The average oxygen loss during our "gentle" plasma exposure is $76 \pm 9 \times 10^{19}$ O atoms/m^2. This oxygen areal density corresponds to 13.5 nm of stoichiometric WO_3. With a total applied D fluence of 1.4×10^{24} D atoms/m^2 this yields an oxygen loss rate of $(5.4 \pm 0.7) \times 10^{-4}$ O atoms per incident D.

Under the assumption that the thin natural oxide film is removed in the same fashion and with the same speed as the thermally grown oxide films, it would take $1.6 \pm 0.4 \times 10^{23}$ D/m^2 to remove the natural oxide film during plasma exposure under the given conditions, i.e., ≈ 10% of the fluence applied in this experiment. Therefore, it can be assumed that the natural oxide is fully removed during the early phase of the D plasma exposure.

3.1.3. Oxygen depth profile

The RBS spectrum of the thick (initially 55 nm) oxide after plasma exposure is shown in Fig. 8. The measurement was performed with 800 keV ^{4}He ions under an incidence angle of 70.5°. The experimental spectrum is shown in red and the simulated spectrum from SIMNRA in blue. A detailed explanation of the interpretation of such RBS spectra is given in Section 2.5. In Fig. 4, an RBS spectrum of the oxide layer before plasma exposure is shown for comparison. The distinct difference before and after plasma exposure is a peak at about 730 keV. This peak can be described by a higher local W concentration at the surface-near region of the oxide film after plasma exposure. For comparison, the simulated spectrum of a WO_3 sample without W enrichment at the surface is shown as a gray dashed line. This W enrichment proofs that the removal of oxygen by the D plasma starts at the surface of the oxide film.

For the high energy part of the RBS spectrum (shaded in green in Fig. 8), the backscattered He ions all stem from within the oxide film on all grains. No He ions detected in this energy interval reached the metallic W underneath. This region, nearest to the surface of the oxide film, can, therefore, be directly modelled without the need for further assumptions of the oxide thickness distribution. For the area shaded in red in Fig. 8, the W grain-dependent thickness variation [35] of the thermally grown oxide needs to be taken into account (see Sections 2.2 and 2.5 for details). For comparison, the simulated spectrum of a WO_3 sample without grain-dependent roughness is shown as a gray dashed line in addition. As most grains are close to the maximum in the thickness distribution, the difference between the two simulations is most pronounced for the deep part of the oxide layer. However, due to technical limitations in the program SIMNRA a layer that incorporates a thickness distribution cannot be further divided into sublayers. Therefore, the area shaded in red can only be represented as a single layer of constant elemental composition in the oxygen depth profiles. However, as the relevant changes in oxygen concentration during plasma exposure appear only in the green-shaded area of the RBS spectrum (near surface region of the oxide film), this will not affect data interpretation. Finally the gray-shaded area in Fig. 8 marks the metallic W substrate underneath the oxide film.

In the following, the oxygen depth profiles derived from the RBS spectra of all samples are presented. The color code of the background is

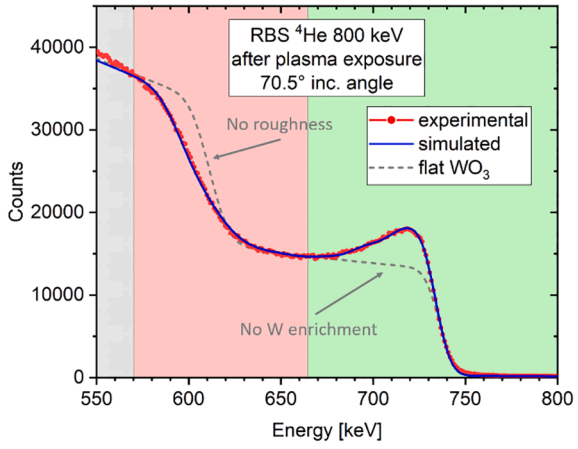

Fig. 8. Experimental (red) and simulated (blue) RBS spectrum for the thick oxide film after plasma exposure. The peak at about 730 keV shows the W enrichment in the surface-near region of the oxide film. The background colors indicate the following parts of the spectrum: green: surface-near region of the oxide where the oxide thickness distribution has no effect on the RBS signal; red: Deeper region of the oxide, where the RBS signal is influenced by oxide thickness distribution; gray: underlying W substrate.

the same as used for Fig. 8. The area shaded in red is always represented by a single layer of constant composition, whereas the area shaded in green allows depth resolved steps. The steps have equal thickness ($50x10^{19}$ atoms/m^2) that is determined by the depth resolution of the RBS measurement in the oxide film. The upper axis of the plot shows the (approximate) thickness of the layers in nm under the assumption of stoichiometric WO_3 with a density of 7.16 g/cm^2. For the W enriched zones in Fig. 9b) and c) this thickness scale is no longer accurate and serves only as an approximate frame of reference.

Fig. 9a) shows the oxygen depth profile of the thick (55 nm) oxide before plasma exposure. It is derived from the RBS spectrum shown in Fig. 4. The W concentration is shown in red and the O concentration in blue. It is evident that the thick oxide film before plasma exposure can be described by WO_3 (i.e., 25 at.% W and 75 at.% O) over its full depth of 385×10^{19} atoms/m^2. After this, the metallic W begins. The slight increase of oxygen at the very surface (by about 1 at.%) can be attributed to a small mismatch of the simulation and the experimental spectrum. The background of the RBS measurement (Fig. 4) increases slightly stronger towards lower energies than predicted by the simulation, possibly due to electronic noise in the detector readout electronics, leading to a slightly higher O content near the surface (high-energy side in the spectrum). In any case, this O increase is barley significant. The error of the W and O concentration in the depth profile was derived by manually varying the concentration and the solid angle of the detector around the fitted values until obvious mismatch between the simulated and the experimental RBS spectra occurred. With this method, the error in the concentration is estimated to be <1 at.%.

Fig. 9b) in turn shows the oxygen depth profile that is derived from the RBS measurement for the thick oxide sample after plasma exposure shown in Fig. 8. It is evident that the W concentration of about 40 at.% at the surface is significantly higher than the 25 at.% expected for stoichiometric WO_3. The W concentration then decreases across the first part of oxide film and reaches the nominal 25 at.% at a depth of about 100×10^{19} atoms/m^2 (which corresponds to roughly 13.5 nm of pure WO_3). This shows that the oxide removal by the D plasma starts at the surface and most probably penetrates with increasing plasma fluence from the surface into the bulk. It definitely does not occur homogeneously throughout the bulk of the oxide film. Due to the limited depth resolution of the RBS measurement, it is not possible to determine if the oxygen concentration increases gradually across this first part or if there is an abrupt jump in concentration. It can, however, be excluded that WO_3 is fully reduced to metallic W at the surface before the oxygen loss can progress deeper into the oxide film. Such behavior would lead to a region of fully reduced metallic W at the surface with intact WO_3 underneath, but simulations of this case deviate strongly from the experimental spectrum in Fig. 8 - even if one assumes that this layer of pure W would form natural oxide on top again after the plasma exposure The measured spectrum (and the same is true for the not shown RBS spectrum belonging to Fig. 9c) is much better represented by the simulation if it is assumed that a partial reduction of the W oxide takes place across the first 100×10^{19} atoms/m^2 (≈13.5 nm) of the oxide film. When comparing this range to the D ion implantation depth in WO_3 for our energies (0.7 nm for 5 eV/D to 1.6 nm for 15 eV/D as obtained with SDTrimSP (version 6.00) [51] from average implantation depth plus a two σ interval), it becomes clear that the kinetic energy of the incident D ions cannot be the immediate cause for the removal of oxygen from the film. Details about these static SDTrimSP calculations can be found in the supplementary material (S4).

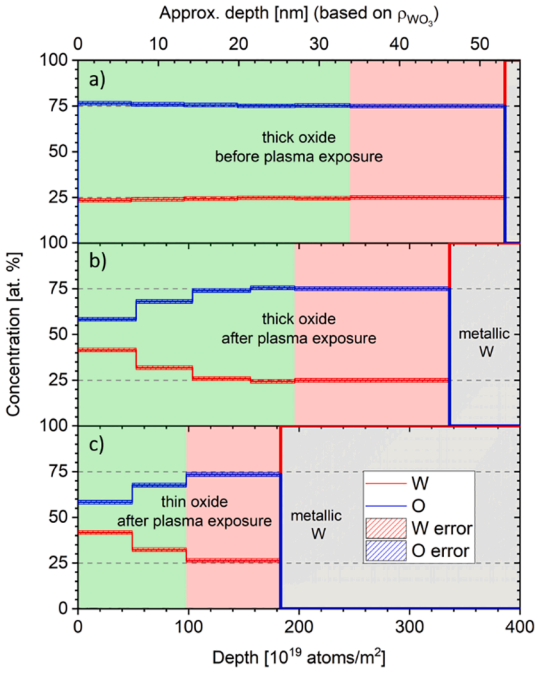

Fig. 9. Oxygen depth profiles derived from 800 keV ^{4}He RBS measurements: a) Thick oxide before plasma exposure (from the RBS spectrum shown in Fig. 4). b) Thick oxide after plasma exposure (from the RBS spectrum shown in Fig. 8). c) Thin oxide after plasma exposure (RBS spectrum not shown). The color code for the background is the same as in Fig. 8.

Fig. 9c) shows the RBS oxygen depth profile of the thin oxide after plasma exposure. Here, the same trend as in Fig. 9b) is visible. At the surface, the W concentration is also increased to about 40 at.%. In the next layer, it is closer to the nominal value of 25 at.% for WO_3. The deeper region of the oxide film can still be well described by stoichiometric WO_3. This part of the oxide film thus appears almost unaltered after plasma exposure, which matches the results of the thick oxide film. This shows that the removal of oxygen from the surface near region of the oxide films is identical in both cases and is independent of the film thickness.

This partial oxygen loss in the near surface region of the thermally grown oxide films during D plasma exposure agrees with previous experiments by Alimov et al. [18]. They have observed a thicker W enrichment zone in the first 130 nm of 1–3 μm thick, thermally oxidized WO_3 layers at plasma exposure temperatures between 340 K and 515 K. They used a total D fluence of 10^{26} D/m^2, a D flux of 10^{22} D/m^{2}s and an energy of 38 eV/D. Despite all three critical parameters that could influence the thickness of the W enrichment zone being one (or in case of the D fluence two) orders of magnitude larger than in our case they observed an increase of only a factor of ten (130 nm compared to 13 nm in our experiments). This is interesting as one could assume that the difference in energy (38 eV/D vs. 5 eV/D) and consequently the deeper implantation of D into the oxide film, would already be enough to explain most of this increase. Furthermore, the 1–3 μm thick oxide layer in the work of Alimov et al. exhibited strong cracking due to the different densities of W oxide and metallic W. These cracks, might also cause a deeper oxygen loss zone compared with our thin, crack-free oxide films. All this implies that the depth-progression of the oxygen loss saturates or at least slows down drastically with increasing D fluence; possibly due to the growing W-enriched layer on top of the oxide film. Further studies of the oxygen loss rate with longer D plasma exposure times under our experimental conditions are needed to address this effect quantitatively.

A further interesting question is which mechanism leads to the oxygen loss and the W enrichment at the surface of the oxide film. We can exclude preferential sputtering of the O atoms by the D plasma as the sole driver of this, because the overall depth of the oxygen loss region of $100 \pm 10 \times 10^{19}$ atoms/m^2 (corresponding to 13.5 nm of stoichiometric WO_3 or 4 nm of metallic W) is much larger than the D ion implantation depth (1.6 nm for 15 eV/D). Sputtering of atoms beyond the D implantation depth is not possible and, as the energy of the D atoms is far too small to allow direct sputtering of W atoms, the W enrichment at the surface would quickly prevent further removal of atoms from the surface.

Another possibility for the oxygen loss could be that (after the first step of chemical reduction of WO_3 by D atoms under formation of deuterium tungsten bronze (D_xWO_3)) a second chemical reaction takes place that forms oxygen-containing molecules that become mobile within the oxide film. However, as the diffusion of D in the WO_3 layer is expected to be high [18,49,50], it is likely that chemical reduction of the tungsten oxide by diffusing D takes place across the full depth of the oxide film, as is indicated by the fast color change of the oxide film that we observed during D plasma exposure (see above). Therefore, we can exclude chemical reduction by D atoms (formation of D_xWO_3) as the rate-limiting mechanism of oxygen loss, because it would lead to a uniform removal of oxygen across the full depth of the oxide film and not only close to the surface.

Thus, we propose the following as a possible mechanism for the oxygen loss in the near-surface region of the oxide film: While in a first step the reduction of WO_3 by D takes place across the full oxide film, the rate-limiting step is the diffusion of O-containing molecules from the place of reduction to the surface. The oxygen loss from the sample is then driven either by thermal or ion-induced desorption from the surface. This can, however, not be fully clarified by this study and further investigations at different energies and/or temperatures are needed.

3.2. Deuterium uptake through surface oxide films and D retention in the film itself

Fig. 10 shows the deuterium depth profiles measured with NRA for all three plasma-exposed samples. The uncertainty of the D concentrations in the D depth profiles is estimated by a post-Markov procedure applied to the data after deconvolution with NRADC. This procedure is described in [6] and gives an asymmetric 1-σ confidence interval of the D concentration around the median concentration for each sublayer of the target (see Section 2.5 for details of the deconvolution with NRADC). The error of the total D areal density in the sample, however, is not determined by the deconvolution but by the uncertainty in the cross section of $<\pm 5\%$ [44,45]. For the small D amounts in the oxidized samples additionally the statistical uncertainty due to counting statistics has to be included, which yields a combined uncertainty of $<\pm 7\%$ in these cases.

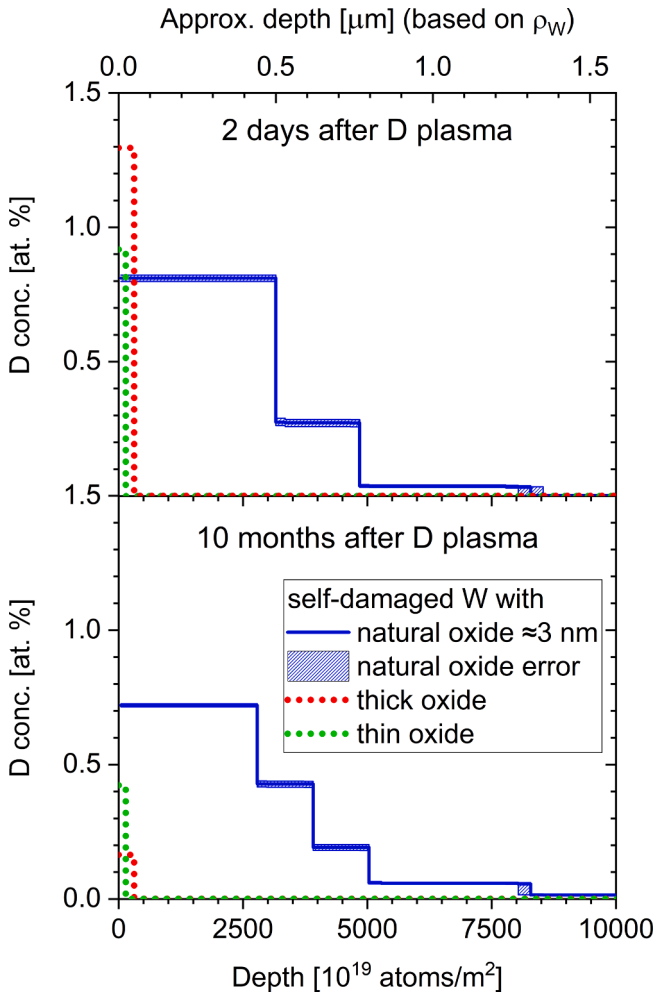

Fig. 10. Deuterium depth profiles measured with NRA. a) Depth profiles two days after plasma exposure. b) Depth profiles ten months after plasma exposure.

Fig. 10a) shows the D depth profiles two days after plasma exposure. The blue line represents the D concentration profile in the reference sample. This sample has only a 2 to 5 nm thick natural oxide film. The areal density of D retained in the reference sample is $31.9 \pm 1.6 \times 10^{19}$ D/m^2. Its D concentration profile extends about 1.3 μm deep into the self-damaged W, but does not completely fill it (the self-damaged W layer is about 2.3 μm thick). This is an expected outcome, as it reproduces the results of similar experiments under these conditions that previously have been conducted in our group [3,7,25]. This further confirms the results of these earlier experiments and indicates that our sample-preparation and plasma-loading procedures are reproducible.

The D depth profiles of the samples with thick and thin oxide two days after plasma exposure are depicted in red and green in Fig. 10a), respectively. They both exhibit only a single D-containing layer close to the surface with no measurable amounts of D deeper in the samples. The depth resolution of the NRA deuterium depth profiling in a WO_3 layer is approx. 50 nm at the surface (see Section 2.4), which is in the order of the oxide thickness for the thick oxide (initially 55 nm). Thus, we can directly confirm that the D in the surface peak of the thick oxide (red in Fig. 10a)) is located solely within the oxide film. For the thin oxide film (initially 33 nm; green in Fig. 10a)), the depth resolution of NRA is larger than the film thickness and consequently this conclusion cannot be directly drawn from the NRA measurement. However, it is quite reasonable to assume, that also for the thin oxide layer D is retained only within the oxide. This is likely, because a) the amount of D in the surface peak is too large to result solely from a monolayer of D surface coverage and b) if D could penetrate through the oxide into the self-damaged W, the D concentration would extend deeper into the sample, which would be clearly visible in the D depth profile and also in the NRA spectrum itself (not shown).

Due to the limited depth resolution of NRA it is not possible to determine a depth profile of the D concentration within the oxide film itself. Therefore, it is not possible to conclude from the NRA depth profiles alone, if the D concentration within the oxide film is distributed homogeneously or if it has a gradient throughout the layer. Nevertheless, assuming a homogenous distribution of D within the oxide film seems reasonable, considering that D is mobile within WO_3 at room temperature (see Section 3.3) [49,50]. This assumption is further supported by Alimov et al. [18] who found D diffusion in thick WO_3 oxide films over several μm already at temperatures of 340 K, i.e., lower than the 370 K used in our experiment. Therefore, in Fig. 10a) the D concentrations in the thermally grown oxide films (green and red) are shown as dotted lines under the assumption of homogeneous D distribution within the oxide films. They should, however, be considered only as a guide for the eye, because the exact thickness of the oxide film after plasma exposure cannot be determined, due the partial oxygen removal by the plasma (see Section 3.1). The D concentration under this assumption is 1.3 at.% for the thick oxide and 0.9 at.% for the thin one. The difference may be an indication that the D is predominantly retained in the stoichiometrically unaffected part of the oxide film that consist still of WO_3 after plasma exposure. The fraction of this unaffected zone relative to the total thickness of the film is bigger for the thick oxide.

Independent of the D distribution within the oxide films, the absolute D areal density in these surface layers can be determined very precisely

by the NRA measurement. The areal density in the oxide film is 4.02 ± 0.28 × 10^{19} D/m^2 for the thick oxide and 1.30 ± 0.09 × 10^{19} D/m^2 for the thin one. The fact that the D retention in the thin oxide is disproportionally smaller than in the thick oxide, again suggests that the D is predominantly retained in the remaining, stoichiometrically unaffected WO_3 deep in the oxide layer. When comparing the amount of this remaining WO_3 for the two oxide films (see Fig. 9b) and 9c)), it is obvious that the thick oxide film has about three times more WO_3 left than the thin oxide film. This corresponds very well to the difference in D retention in the two oxide films. In any case, the absolute D retention in the oxidized samples is significantly smaller (factor of 8 and 25 for the thick and thin oxide, respectively) than in the reference sample with only natural oxide that shows a retention of 31.9 ± 1.6 × 10^{19} D/m^2.

Thus, the D depth profiling with NRA clearly shows that oxide films of initially 33 and 55 nm thickness effectively block D diffusion into the (self-damaged) metallic W. This is a new and unexpected result, as there is very little data available in the literature on D uptake in W through surface oxide films. There is one study by Ogorodnikova et al. [19] who claims that D is retained deep in the bulk W beyond a WO_3 film of 100 to 400 nm thickness for thermally oxidized W samples after irradiation with D ions at an energy of 200 eV. This statement relies on a sole measurement of the D concentration in the sample with ^{3}He NRA at a single energy of 1 MeV which corresponds to a probing depth of about 1 μm depending on the oxide thickness. However, with only one single energy and the detector setup used in [19], no depth profiling of the D concentration in the sample can be achieved. It is, therefore, not clear to us, how this measurement can yield information on whether the D is located inside or beyond the oxide layer.

From our detailed RBS and NRA depth profiling with energies from 0.5 to 4.5 MeV and the use of the surface sensitive alpha spectrum, we have obtained a clear and accurate picture of the depth distribution of both the oxygen and the D in the sample. Therefore, we can with certainty say that for the thick oxide any D that is retained in the sample is retained within the oxide film. For the thin oxide, this is also strongly indicated. No D has penetrated through the oxide films into the self-damaged W after the here applied D plasma exposure.

3.3. Long time D retention in the oxide film

The D depth profile of the three plasma-exposed samples (natural oxide, thin and thick oxide) was measured again after a waiting period of ten months. The samples were stored at room temperature in a desiccator under vacuum during this time. The D depth profiles after the waiting period are shown in Fig. 10b).

The D content in the reference sample with the natural oxide (blue) is now 29.8 ± 1.5 × 10^{19} D/m^2 and has stayed about constant with a measured change of –2.1 ± 2.2 × 10^{19} D/m^2 after the waiting period from the initial value of 31.9 ± 1.6 × 10^{19} D/m^2. This small relative difference of about 6.6% is close to the experimental uncertainty. Therefore, none or only a very small amount of D is lost from the natural oxide sample. This was expected, since the D should be firmly trapped in defects in the self-damaged W underneath the natural oxide film and much higher temperatures are needed for a thermal release [3,26]. A similar small reduction (in the order of 5%) of the trapped D amount due to storage in vacuum was also observed in a dedicated study by Wielunska et al. [3].

But more importantly, the deuterium amount in the oxidized samples (red and green) has diminished drastically. From 4.02 ± 0.28 to 0.40 ± 0.03 × 10^{19} D/m^2 (90% reduction) in the case of the thick oxide (red) and from 1.30 ± 0.09 to 0.59 ± 0.04 × 10^{19} D/m^2 (55% reduction) in the case of the thin oxide (green). From the strong reduction of D over time, one can conclude two things: First, the D must be mobile in the oxide at room temperature to be able to leave the oxide. Second, it does leave the oxide towards the surface and not towards the self-damaged W. Otherwise, it would still be detectable by NRA as the defects in the self-damaged W do not release trapped D at room temperature (see above).

The first conclusion is already well known in literature, see e.g. [20]. The second conclusion, however, is new. We interpret our results as follows: Tungsten oxide films acts as a permeation barrier for D into W. This holds true even after a waiting period of ten months at room temperature in vacuum. However it is not the limited transport within the oxide that prevents permeation but the D is stopped at the interface to the metallic W. Based on our current knowledge of the system, we propose the following model assumption as a possible explanation for this behavior: During plasma loading D is implanted beneath the surface into the oxide film (mean implantation range 0.7 nm for 5 eV/D), where it is thermalized to the sample temperature (370 K). Within minutes [50], it diffuses throughout the full depth of the oxide film up to the interface under the formation of deuterium tungsten bronze (D_xWO_3). In contrast to a direct, plasma-driven implantation into the metallic W, the thermalized D in the oxide film does not possess enough energy to overcome the difference in the enthalpy of solution (Q_{Sol}) between WO_3 and metallic W. This is schematically illustrated in Fig. 11. The exact height of this barrier is not known, but can be estimated by two additional pieces of information: 1) The difference in the enthalpy of solution between vacuum and metallic W for D atoms is in the order of 1.04 to 1.14 eV [21,52]. 2) HIs can be absorbed in WO_3 from a HI-rich atmosphere at temperatures above 394 K [53] (see activation barrier indicated in Fig. 11). Additionally, they can desorb again into vacuum at room temperature over a timescale of months. Therefore, the enthalpy of solution of D in WO_3 must be slightly positive (above that of D_2 in vacuum) but well below that of D in W. Consequently, the difference in the enthalpy of solution for D atoms in WO_3 and in W should be close to 1 eV. This energy difference is too high to be overcome by the D atoms in WO_3 in our experiment at 370 K. Note that the energy necessary for a diffusion step ΔE_{diff} for hydrogen in WO_3 is stated as 0.35 eV from DFT calculations in [54] and as 0.4 eV from experiments in [55]. For metallic tungsten ΔE_{diff} for hydrogen and D is stated as 0.28 ± 0.06 in [22] and as 0.39 eV in [21].

One can assume that the thin (2–3 nm) natural oxide film, always present in many laboratory experiments, exhibits the same behavior and reduces or even prevents the D transport into metallic W at low temperature. Since the sample with the natural oxide showed significant D concentration in the self-damaged layer, however, it can be concluded that this effect only lasts until the natural oxide film is either fully removed by the plasma or at least reduced below the maximum D ion implantation range (1.6 nm for 15 eV/D (3% of D ions in the present

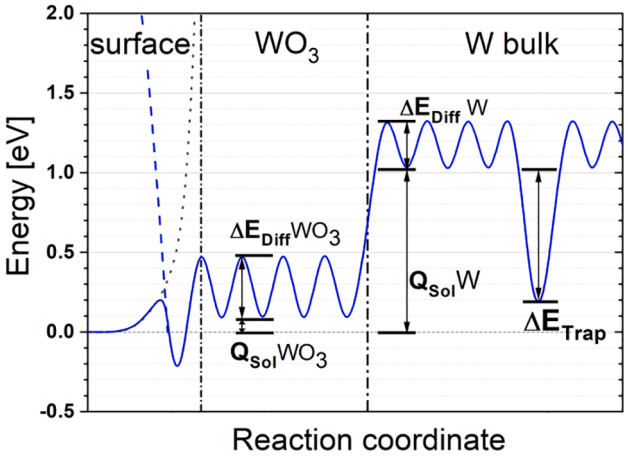

Fig. 11. Schematic representation of the energy landscape of D in WO_3 and W. The dashed line at the surface marks the energy of a D atom. The dotted gray line marks the repulsive potential for the D_2 molecule close to the surface. The heat of solution (Q_{sol}) and the energy necessary for a diffusive step (ΔE_{Diff}) for WO_3 and W are shown. In the (self-damaged) W bulk also a D trap with trapping energy ΔE_{Trap} is shown. A detailed discussion of the absolute values is provided in the text.

case) or 0.7 nm for the majority species of 5 eV/D (96% of D ions)). Under the assumption that the thin natural oxide film is removed in the same fashion and with the same speed as the thermally grown oxide films, a full removal is expected to take place within the first 10% of the plasma exposure time/D fluence applied in this work (compare Section 3.1.2). After the natural oxide is removed the D ions can be directly implanted into the W bulk as their energy is high enough to overcome the enthalpy of solution in W (1.04 to 1.14 eV [21,22]). Note, that the natural oxide film is reformed after plasma exposure, when the sample is again exposed to ambient atmosphere. In case of the samples with thermally grown oxide films (initially 33 and 55 nm), only a partial oxide removal takes place in the surface near region (first 100 $\times$ 10^{19} atoms/m^2). In larger depths, especially at the interface between oxide and metallic tungsten, the stoichiometric composition of WO_3 is still intact.

It is worth mentioning that the proposed barrier mechanism acts only in one way. While the uptake of D from the WO_3 into the metallic W is reduced or blocked, the transport in the opposite direction should not be affected. The present experiments allow only to draw conclusion in one direction for the D uptake. However, to interpret thermo-desorption data the influence of thin tungsten oxide films on D desorption from tungsten has to be known. Presently investigations are under way to address this issue.

4. Summary and conclusion

D uptake experiments through thin surface oxide films on W samples have been carried out. A 2.3 μm thick layer of self-damaged W underneath the oxide was used as a getter layer to trap D atoms possibly penetrating the oxide film. The oxide was thermally grown in a mixture of 80% Ar and 20% O_2 at 600 K to thicknesses of 33 nm and 55 nm. D was supplied by a "gentle" (<5 eV/D) D plasma at 370 K.

It was found that the thermally grown oxide films take up substantial amounts of D. By nuclear reaction analysis, D concentrations in the order of 1 at. % within the oxide film were determined. This was an expected result, as the high D retention inside tungsten oxide is well known in literature [18,56]. However, despite the high D retention in the tungsten oxide itself, the oxide film effectively blocks the D transport into the (self-damaged) W. No D was found in the W beneath the thermally grown oxide films. This is a new and important result as it indicates that tungsten oxide films form an effective permeation barrier for D transport into metallic W. We propose the following model assumption as a possible explanation for this behavior: D is thermalized inside the oxide film at the plasma exposure temperature of 370 K and cannot overcome the difference in the heat of solution between W oxide and metallic W. Note, however, that this is expected to be a diode-like, one way D uptake barrier, as there is no indication that D uptake from W to W oxide would be blocked.

Furthermore, it is evident from our experiments that oxygen is partially removed from the near surface region of the oxide film by the D plasma. With RBS measurements, an enrichment of W in the near-surface region of the oxide film was found. A deuterium fluence of 1.4×10^{24} D/m^2 over seven hours of exposure time lead to a removal of $76 \pm 6 \times 10^{19}$ O atoms/m^2 (corresponding to about 13.5 nm of WO_3, which contains the W amount of $\approx$ 4 nm of metallic W). Furthermore, the O removal appears to be independent of the original oxide thickness. These two findings show that the reduction starts from the surface and is not a volume effect. From analysis of the RBS data it is obvious that the W surface enrichment cannot be explained by a single ($\approx$ 4 nm thick) layer of metallic tungsten on top of the oxide layer. This holds true even when one assumes that this layer of pure W would form natural oxide on top again after the plasma exposure. The oxygen depth profile derived from RBS suggests that this partially oxygen depleted zone stretches 100 $\times$ 10^{19} atoms/m^2 ($\approx$ 13.5 nm) deep into the oxide film. It consists of W oxide with up to 40 at.% of W at the surface and gradually returns to stoichiometric WO_3 (25 at.% W) with increasing depth. Thus, the W enriched zone extends far deeper than the D implantation depth in the oxide, which is smaller than 2 nm for the D energies used in our experiments.

Finally, the D depth profile measurement (with NRA) was repeated after ten months of storage time in a desiccator. During this time, most of the D stored in the oxide films escaped into the vacuum.

As a conclusion, it is evident that thermally grown WO_3 layers on W

a) take up D atoms from the plasma quickly and homogenously throughout the film under the formation of deuterium tungsten bronze (D_xWO_3),
b) prevent further transport into the underlying metallic W substrate due to the difference in the heat of solution in W oxide and metallic W; i.e., the interface of WO_3/W acts as a transport barrier
c) are (slowly) removed by the plasma starting from the surface even at 370 K and low energies of < 5 eV / D,
d) release D on a timescale of several months at room temperature.

One can assume that the thin (2–5 nm) natural oxide film, always present in many laboratory experiments, exhibits the same behavior and reduces or even prevents the D transport into metallic W until it is removed by the plasma. This possible influence of the natural oxide film on D uptake into metallic W needs to be considered when evaluating D uptake and *permeation* experiments, e.g. [8], in order to draw the right conclusions for un-oxidized W. The effect is expected to be especially prominent for experiments with low plasma fluence or fluence series where the sample has contact with air in between plasma exposures.

Furthermore, we expect an effect of the sample temperature on the removal rate of the oxide and thus on the D fluence that is necessary to fully remove the oxide film and enable D entering the bulk. Higher temperatures might also enable a diffusion from the oxide film into the self-damaged W [57]. The higher thermal energy of the D atoms could then enable a jump across the energy step due to the difference in the enthalpy of solution at the WO_3/W interface. In addition, the D ion energy and D ion flux might play an important role on the oxygen removal rate. Further studies with an extended set of parameters are planned to draw a comprehensive picture of the energy, flux and temperature dependence of a) the oxide removal efficiency, b) the retention of D in the oxide and c) the transport of D into the metallic W. For high D energies, we expect some D ions to be implanted directly into the metallic W beneath the oxide film, which would circumvent the permeation barrier effect of the W oxide/W interface.

CRediT authorship contribution statement

Kristof Kremer: Investigation, Formal analysis, Data curation, Validation, Writing - original draft, Visualization. **Thomas Schwarz-Selinger:** Conceptualization, Methodology, Resources, Validation, Data curation, Writing - review & editing, Supervision. **Wolfgang Jacob:** Data curation, Validation, Writing - review & editing, Project administration.

Declaration of Competing Interest

The authors declare that they have no known competing financial interests or personal relationships that could have appeared to influence the work reported in this paper.

Acknowledgements

We thank Joachim Dorner and Michael Fusseder for operating the tandem accelerator and Armin Manhard for providing and maintaining the PlaQ setup. We greatly appreciate the support and assistance of Martin Balden and Stefan Elgeti with the SEM imaging and the FIB cross sections and thank Matej Mayer for his counsel on the SIMNRA modelling of the RBS and NRA measurements and Klaus Schmid for his counsel

on NRADC. We thank Katja Hunger for the help with grinding and polishing, Karsten Schlüter for the help with thermal oxidation and for providing the W grain-dependent oxide thickness distribution prior to publication and Till Höschen for performing the XPS measurements. Lastly, we thank Ulrich Stroth for his fruitful discussion and interest in this work.

Appendix A. Supplementary data

Supplementary data to this article can be found online at https://doi.org/10.1016/j.nme.2021.100991.

References

[1] J. Roth, et al., Recent analysis of key plasma wall interactions issues for ITER, J. Nucl. Mater. 390–391 (2009) 1–9, https://doi.org/10.1016/j.jnucmat.2009.01.037.
[2] W.R. Wampler, R.P. Doerner, The influence of displacement damage on deuterium retention in tungsten exposed to plasma, Nucl. Fusion 49 (11) (2009), 115023, https://doi.org/10.1088/0029-5515/49/11/115023.
[3] B. Wielunska, et al., Deuterium retention in tungsten irradiated by different ions, Nucl. Fusion 60 (2020) 096002, https://doi.org/10.1088/1741-4326/ab9a65.
[4] T. Schwarz-Selinger, et al., Influence of the presence of deuterium on displacement damage in tungsten, Nucl. Mater. Energy 17 (2018) 228–234, https://doi.org/10.1016/j.nme.2018.10.005.
[5] S. Kapser, et al., Influence of sub-surface damage evolution on low-energy-plasma-driven deuterium permeation through tungsten, Nucl. Fusion 58 (5) (2018), 056027, https://doi.org/10.1088/1741-4326/aab571.
[6] M. Zibrov, et al., Deuterium trapping by deformation-induced defects in tungsten, Nucl. Fusion 59 (10) (2019) 106056, https://doi.org/10.1088/1741-4326/ab3c7e.
[7] J. Bauer, et al., Influence of near-surface blisters on deuterium transport in tungsten, Nucl. Fusion 57 (8) (2017), 086015, https://doi.org/10.1088/1741-4326/aa7212.
[8] S. Kapser, A. Manhard, U. von Toussaint, Measuring deuterium permeation through tungsten near room temperature under plasma loading using a getter layer and ion-beam based detection, Nucl. Mater. Energy 12 (2017) 703–708, https://doi.org/10.1016/j.nme.2016.11.019.
[9] S. Markelj, et al., Displacement damage stabilization by hydrogen presence under simultaneous W ion damage and D ion exposure, Nucl. Fusion 59 (8) (2019), 086050, https://doi.org/10.1088/1741-4326/ab2261.
[10] M.J. Simmonds, et al., Isolating the detrapping of deuterium in heavy ion damaged tungsten via partial thermal desorption, J. Nucl. Mater. 522 (2019) 158–167, https://doi.org/10.1016/j.jnucmat.2019.05.016.
[11] D. Schneider, et al., Ergänzungsband Teil B 1. Die Systeme mit Edelgasen, in: Wasserstoff und Sauerstoff, Springer-Verlag, Berlin Heidelberg, 1978.
[12] C.H. Skinner, et al., Recent advances on hydrogen retention in ITER's plasma-facing materials: beryllium, carbon, and tungsten, Fusion Sci. Technol. 54 (4) (2008) 891–945, https://doi.org/10.13182/FST54-891.
[13] R.A. Causey, Hydrogen isotope retention and recycling in fusion reactor plasma-facing components, J. Nucl. Mater. 300 (2–3) (2002) 91–117, https://doi.org/10.1016/S0022-3115(01)00732-2.
[14] E.A. Hodille, et al., Retention and release of hydrogen isotopes in tungsten plasma-facing components: the role of grain boundaries and the native oxide layer from a joint experiment-simulation integrated approach, Nucl. Fusion 57 (7) (2017), 076019, https://doi.org/10.1088/1741-4326/aa6d24.
[15] C. Hopf, W. Jacob, V. Rohde, Oxygen glow discharge cleaning in nuclear fusion devices, J. Nucl. Mater. 374 (3) (2008) 413–421, https://doi.org/10.1016/j.jnucmat.2007.10.001.
[16] S.K. Deb, Opportunities and challenges in science and technology of WO_3 for electrochromic and related applications, Sol. Energy Mater. Sol. Cells 92 (2) (2008) 245–258, https://doi.org/10.1016/j.solmat.2007.01.026.
[17] M.H. Yaacob, et al., Absorption spectral response of nanotextured WO_3 thin films with Pt catalyst towards H_2, Sens. Actuators B Chem. 137 (1) (2009) 115–120, https://doi.org/10.1016/j.snb.2008.12.035.
[18] V.K. Alimov, et al., Surface morphology and deuterium retention in tungsten oxide layers exposed to low-energy, high flux D plasma, J. Nucl. Mater. 409 (1) (2011) 27–32, https://doi.org/10.1016/j.jnucmat.2010.12.028.
[19] O.V. Ogorodnikova, J. Roth, M. Mayer, Deuterium retention in tungsten in dependence of the surface conditions, J. Nucl. Mater. 313–316 (2003) 469–477, https://doi.org/10.1016/S0022-3115(02)01375-2.
[20] Y. Addab, et al., Formation of thin tungsten oxide layers: characterization and exposure to deuterium, Phys. Scr. T167 (2016), 014036, https://doi.org/10.1088/0031-8949/T167/1/014036.
[21] R. Frauenfelder, Solution and diffusion of hydrogen in tungsten, J. Vac. Sci. Technol. 6 (3) (1969) 388–397, https://doi.org/10.1116/1.1492699.
[22] G. Holzner, et al., Solute diffusion of hydrogen isotopes in tungsten—a gas loading experiment, Phys. Scr. T171 (2020), 014034, https://doi.org/10.1088/1402-4896/ab4b42.
[23] PLANSEE Metall GmbH – High Performance Materials, PLANSEE, A-6600-Reutte, Austria, http://www.plansee.com.
[24] A. Manhard, G. Matern, M. Balden, A step-by-step analysis of the polishing process for tungsten specimens, Pract. Metallogr. 50 (1) (2013) 5–16, https://doi.org/10.3139/147.110215.
[25] T. Schwarz-Selinger, Deuterium retention in MeV self-implanted tungsten: Influence of damaging dose rate, Nucl. Mater. Energy 12 (2017) 683–688, https://doi.org/10.1016/j.nme.2017.02.003.
[26] E.A. Hodille, et al., Stabilization of defects by the presence of hydrogen in tungsten: simultaneous W-ion damaging and D-atom exposure, Nucl. Fusion 59 (1) (2019), 016011, https://doi.org/10.1088/1741-4326/aaec97.
[27] E. Markina, et al., Recovery temperatures of defects in tungsten created by self-implantation, J. Nucl. Mater. 463 (2015) 329–332, https://doi.org/10.1016/j.jnucmat.2014.12.005.
[28] M. Zibrov, et al., High temperature recovery of radiation defects in tungsten and its effect on deuterium retention, Nucl. Mater. Energy 23 (2020), 100747, https://doi.org/10.1016/j.nme.2020.100747.
[29] F. Y. Xie, XPS studies on surface reduction of tungsten oxide nanowire film by Ar+ bombardment, J. Electron Spectrosc. Relat. Phenom., V. 185, p. 7, 2012, https://doi.org/10.1016/j.elspec.2012.01.004.
[30] C. Martin, et al., Tungsten oxide thin film bombarded with a low energy He ion beam: evidence for a reduced erosion and W enrichment, Phys. Scr. T170 (2017), 014019, https://doi.org/10.1088/1402-4896/aa89c1.
[31] E. Lassner, W.-D. Schubert, Tungsten: Properties, Chemistry, Technology of the Element, Alloys, and Chemical Compounds, Springer, US, Boston, MA, 1999.
[32] A. Paliwal, et al., Optical properties of WO_3 thin films using surface plasmon resonance technique, J. Appl. Phys. 115 (4) (2014), 043104, https://doi.org/10.1063/1.4862962.
[33] G. Fulton, A. Lunev, Probing the correlation between phase evolution and growth kinetics in the oxide layers of tungsten using Raman spectroscopy and EBSD, Corros. Sci. 162 (2020), 108221, https://doi.org/10.1016/j.corsci.2019.108221.
[34] K. Schlueter, M. Balden, Dependence of oxidation on the surface orientation of tungsten grains, Int. J. Refract. Met. Hard Mater. 79 (2019) 102–107, https://doi.org/10.1016/j.ijrmhm.2018.11.012.
[35] Personal Communication with Karsten Schlüter at IPP Garching, Boltzmannnstraße 2, 85748 Garching by Munich.
[36] A. Manhard, T. Schwarz-Selinger, W. Jacob, Quantification of the deuterium ion fluxes from a plasma source, Plasma Sources Sci. Technol. 20 (1) (2011), 015010, https://doi.org/10.1088/0963-0252/20/1/015010.
[37] A. Manhard, M. Balden, U. von Toussaint, Blister formation on rough and technical tungsten surfaces exposed to deuterium plasma, Nucl. Fusion 57 (12) (2017), 126012, https://doi.org/10.1088/1741-4326/aa82c8.
[38] M. Mayer, et al., Quantitative depth profiling of deuterium up to very large depths, Nucl. Instr. Meth. B 267 (3) (2009) 506–512, https://doi.org/10.1016/j.nimb.2008.11.033.
[39] Gestis Stoffdatenbank:http://gestis.itrust.de/nxt/gateway.dll/gestis_de/005920.xml?f=templates$fn=default.htm$3.0, Oct. 19, 2020.
[40] M. Mayer, RESOLNRA A new program for optimizing the achievable depth resolution of ion beam analysis methods, Nucl. Instr. Meth. B 266 (8) (2008) 1852–1857, https://doi.org/10.1016/j.nimb.2007.11.071.
[41] J.F. Ziegler, www.srim.org.
[42] M. Mayer, "SIMNRA User's Guide", IPP Report 9/113, Max-Planck-Institut für Plasmaphysik, Garching, 1997, Link: http://hdl.handle.net/11858/00-001M-0000-0027-6157-F.
[43] K. Schmid, U. von Toussaint, Statistically sound evaluation of trace element depth profiles by ion beam analysis, Nucl. Instr. Meth. B 281 (2012) 64–71, https://doi.org/10.1016/j.nimb.2012.03.024.
[44] W. Moller, F. Besenbacher, A note on the ^{3}He+D nuclear-reaction cross section, Nuclear intruments and methods 168 (1980) 111–114, https://doi.org/10.1016/0029-554X(80)91239-2.
[45] B. Wielunska, et al., Cross section data for the D(^{3}He, p) ^{4}He nuclear reaction from 0.25 to 6 MeV, Nucl. Instr. Meth. B 371 (2016) 41–45, https://doi.org/10.1016/j.nimb.2015.09.049.
[46] M. Guitart Corominas, T. Schwarz-Selinger, Experimental determination of the ^{16}O (^{3}He, p_0)^{18}F differential cross section, Nucl. Instr. Meth. B 450 (2019) 13–18, https://doi.org/10.1016/j.nimb.2018.05.018.
[47] https://materialsproject.org/materials/mp-19033/, Nov. 19, 2020.
[48] T.F. Silva, et al., MultiSIMNRA: A computational tool for self-consistent ion beam analysis using SIMNRA, Nucl. Instr. Meth. B 371 (2016) 86–89, https://doi.org/10.1016/j.nimb.2015.10.038.
[49] K. Ito, T. Ohgami, T. Nakazawa, Effect of water on hydrogen-sensitive tungsten oxide films, Sens. Actuators B Chem. 12 (3) (1993) 161–167, https://doi.org/10.1016/0925-4005(93)80014-3.
[50] S. Burkhardt, et al., In situ monitoring of lateral hydrogen diffusion in amorphous and polycrystalline WO_3 thin films, Adv. Mater. Interfaces 5 (6) (2018) 1701587, https://doi.org/10.1002/admi.201701587.
[51] A. Mutzke, et al., SDTrimSP Version 6.00, IPP Report IPP 2019-2, Max-Planck-Institut für Plasmaphysik, Garching, (2019). http://hdl.handle.net/21.11116/0000-0002-F6AE-5.
[52] G. Holzner, Determining fundamental transport parameters of hydrogen isotopes in tungsten, PhD Thesis, 2020, Technical University Munich.
[53] S.J. Ippolito, et al., Hydrogen sensing characteristics of WO3 thin film conductometric sensors activated by Pt and Au catalysts, Sens. Actuators B Chem. 108 (1–2) (2005) 154–158, https://doi.org/10.1016/j.snb.2004.11.092.
[54] H. Lin, et al., Non-Grotthuss proton diffusion mechanism in tungsten oxide dihydrate from first-principles calculations, J. Mater. Chem. A 2 (31) (2014) 12280, https://doi.org/10.1039/C4TA02465F.

[55] J. Randin, R. Viennet, Proton diffusion in tungsten trioxide thin films, J. Electrochem. Soc. 129 (10) (1982) 2349–2354, https://doi.org/10.1149/1.2123510.
[56] A. Inouye, et al., Hydrogen retention induced by ion implantation in tungsten trioxide films, Nucl. Instr. Meth. B 267 (8–9) (2009) 1480–1483, https://doi.org/10.1016/j.nimb.2009.01.139.
[57] A. Založnik, et al., Deuterium atom loading of self-damaged tungsten at different sample temperatures, J. Nucl. Mater. 496 (2017) 1–8, https://doi.org/10.1016/j.jnucmat.2017.09.003.